Optics and Laser Technology 123 (2020) 105941

Contents lists available at ScienceDirect

Optics and Laser Technology

journal homepage: www.elsevier.com/locate/optlastec

Flexible and lightweight speckle noise suppression module based on generation of dynamic speckles with multimode fiber and macro fiber composite

Quan Gao[a,b,1], Zhaomin Tong[a,b,1,*], Yifei Ma[a,b], Mei Wang[a,b], Suotang Jia[a,b], Xuyuan Chen[a,b,c]

[a] State Key Laboratory of Quantum Optics and Quantum Optics Devices, Institute of Laser Spectroscopy, Shanxi University, Taiyuan, Shanxi 030006, China
[b] Collaborative Innovation Center of Extreme Optics, Shanxi University, Taiyuan, Shanxi 030006, China
[c] Faculty of Technology, Natural Sciences and Maritime Sciences, Department of Microsystems, University of Southeast Norway, Borre N-3184, Norway

HIGHLIGHTS

- The speckle reduction module is flexible and lightweight.
- Dynamic speckles are time-averaged during the exposure time of a CCD camera.
- The most efficient speckle reduction condition is obtained.
- High-quality low-speckle projection image in a laser projector is demonstrated.

ARTICLE INFO

Keywords:
Speckle noise suppression
Multimode fiber
Macro fiber composite
Laser displays

ABSTRACT

We propose a flexible and lightweight laser speckle noise suppression module based on the combination of a multimode fiber (MMF) and a macro fiber composite (MFC). The mechanism underlying speckle suppression involves the time-averaging of dynamic speckles during the exposure time of a charge-coupled device, wherein the MFC causes MMF vibration via its fast and periodic stretching due to the piezoelectric effect. The most efficient speckle reduction condition is realized when the MMF is vibrating in a resonant mode under the application of the highest MFC driving voltage and a large MMF effective numerical aperture. We obtain a speckle contrast of 0.08 when this "most efficient" speckle reduction condition is used to illuminate a diffuser. Further, the image quality is improved when our module is applied in a projector, which makes the device a flexible and lightweight module for speckle reduction in laser displays.

1. Introduction

It is well known that in comparison with conventional light sources, lasers can offer the benefits of higher brightness, higher directionality, wider color gamut, longer lifetime, etc. Lasers are widely used in diverse fields such as laser displays [1–3], optical coherence tomography [4], and optical communication [5]. When a laser beam illuminates a rough-surfaced object, interference occurs between the scattered beams because of high coherence, which results in the formation of bright or dark granular patterns called speckles [6]. The appearance of speckles degrades the image quality in laser projection systems [7,8]. In general, speckles can be reduced by the application of polarization diversity [9], angular diversity [10–12], wavelength diversity [12,13], the use of broadband light sources [14,15], rotating diffusers [16], specially designed screens [17], etc.

When a coherent laser beam is guided into a multimode fiber (MMF), a speckle pattern is produced at the output of the MMF because of interference among the guided modes [18]. One speckle reduction method at the output of the MMF involves the enhancement of the modal dispersion of the MMF via increasing its length or numerical aperture (NA) [19,20]. Via splitting of a laser beam into "sub-beams" and guiding these into a fiber bundle with different fiber lengths, speckle can be reduced by destroying the laser radiation temporal coherence by creating a sufficient optical path difference among the fibers [21]. Other approaches involve the tight coiling of the MMF around a cylindrical piezoelectric transducer block or the MMF fixed on a

* Corresponding author.
E-mail address: zhaomin.tong@sxu.edu.cn (Z. Tong).
[1] Both authors contributed equally.

https://doi.org/10.1016/j.optlastec.2019.105941
Received 2 September 2019; Received in revised form 25 October 2019; Accepted 1 November 2019
Available online 08 November 2019
0030-3992/

piezoelectric plate to reduce speckle. The periodic vibration of the piezoelectric block and plate results in subsequent intensity modulation over the MMF, and consequently, the speckles at the output of the MMF are time-averaged and reduced during the integration time of the human eyes [22,23]. However, while these methods are feasible for speckle reduction, the corresponding devices suffer from problems such as the complexity or bulkiness of the setup, which makes it difficult to practically apply them in laser projection systems.

Against this backdrop, here, we demonstrate a flexible and lightweight laser speckle noise suppression module that uses a macro fiber composite (MFC) as a driver to vibrate a MMF. The vibration of the MMF generates dynamic speckle patterns, which can be time-averaged during the exposure time of a charge-coupled device (CCD) camera or the human eyes. In this study, we used two types of MMFs with different NAs and calculated the speckle contrast ratios to compare the speckle reduction efficiencies. The relationships between speckle contrast ratios and the MFC driving frequency and voltage were also studied to determine the optimized driving conditions for the most efficient speckle reduction. The proposed configuration was further utilized as a low-coherence illumination light source in a projector, which afforded high-quality projection images.

2. Structure of MFC

MFCs, which are used as advanced actuators and sensors, offer the benefits of compact size, high performance, flexibility, and reliability [24]. The MFC used in the study was manufactured by Smart Material Corp. (type: M8514-P2). Fig. 1(a) schematically illustrates the structure of the MFC, which consists of three primary components: piezoceramic rods made of lead zirconate titanate, a pair of thin polyimide films (top and bottom) etched with conductive electrodes, and two layers of adhesive matrix material. In order to improve the damage tolerance and flexibility relative to the monolithic ceramic, the aligned rectangular piezoceramic rods (bonded by adhesive matrix material) are sandwiched between the layers of adhesive matrix material and polyimide film. The electrodes are affixed to the film, which transfers the applied voltage directly to the ribbon-shaped rods. The adhesive material bonds the actuator components together. Depending on the poling direction, MFCs are classified as d_{33} and d_{31} types. In d_{31} type MFCs, the poling direction and the electric field are perpendicular to the piezoceramic rod orientation [25]. As shown in Fig. 1(b), the poling direction and the electric field are along the z-axis, and the piezoceramic rod orientation is along the x-axis. Consequently, the d_{31} piezoelectric effect is utilized here. When an electric field is applied, the rods yield a longitudinal deformation due to the d_{31} piezoelectric effect. The MFC generates vibrations owing to its resulting contraction and relaxation when it is driven by a variable voltage such as a sinusoidal waveform. Fig. 1(c) shows the prototype of the packaged MFC, whose overall length and width are 100 mm and 18 mm, respectively. Further, the device thickness is 0.3 mm.

From Fig. 1(c), the high portability and handling ease of the device appears obvious. Considering the advantages and properties of the MFC, it forms an obvious candidate for application as an actuator to induce vibration in MMFs toward the realization of a flexible and lightweight speckle noise suppression module.

3. Theory and experimental setup

3.1. Speckle reduction theory

Speckle contrast ratio C is normally utilized to characterize the speckle effect. Speckle contrast ratio C is defined as [6]

$$C = \frac{(\langle I^2\rangle - \langle I\rangle^2)^{1/2}}{\langle I\rangle} = \frac{\sigma}{\langle I\rangle}, \tag{1}$$

where I, $< I >$, and σ represent the speckle intensity, mean value, and standard deviation of the speckle intensity, respectively.

We used two types of MMFs with different NAs in our experiments, which were designated as fiber A and fiber B. The two fibers are made of different materials, where fiber A is an unjacketed plastic fiber with acrylic core, and fiber B is a jacketed quartz fiber with silica core. The specifications of fibers A and B are listed in Table 1.

Because of modal dispersion in a MMF, the phases of the modes at the output of the MMF are different, which results in a time difference between the earliest and last-to-arrive signal components of the MMF. This time difference $\Delta\tau$ can be defined as [6]

$$\Delta\tau = \frac{L(NA_e)^2}{2cn_1}, \tag{2}$$

where L, NA_e, and n_1 represent the length, effective numerical aperture, and refractive index of core of the MMF, respectively, and c the speed of light in vacuum.

When a laser is coupled into the MMF, the speckle contrast ratio C at the end of the stationary MMF can be expressed as [20]

$$C^2 = \left[1 + \frac{1}{2}\left(\frac{2\pi\Delta\nu\Delta\tau}{3^{1/2}}\right)\right]^{-1/2}, \tag{3}$$

where $\Delta\nu$ represents the Gaussian spectral profile with $1/e$ half-width.

From Eqs. (2) and (3), it is obvious that the speckle contrast reduces with increase in the time difference $\Delta\tau$ of the stationary MMF. In particular, as the modal dispersion is increased, some modes cannot interfere at the output of the MMF because the laser radiation temporal coherence may be lost, which results in a reduction in speckle contrast.

Upon assuming that M modes are guided into the MMF, each of these modes will propagate along the MMF with a specific propagation constant. The guided modes are very sensitive to the external

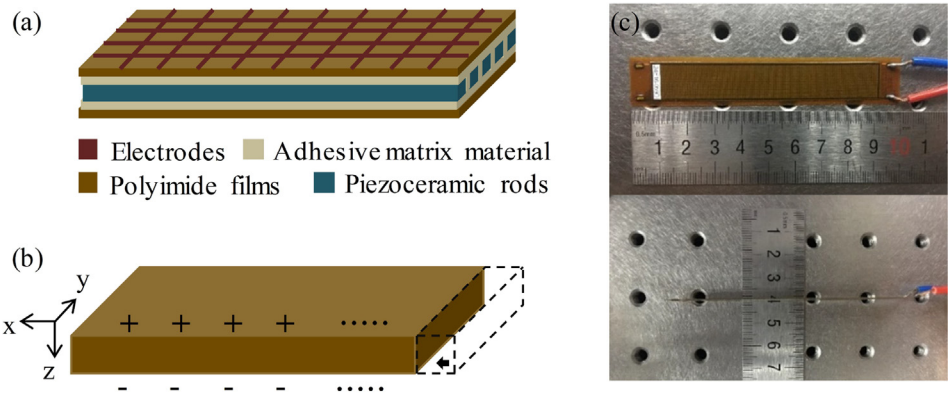

Fig. 1. (a) Structure of macro fiber composite (MFC). (b) MFC longitudinal deformation due to d_{31} piezoelectric effect upon application of driving voltage. (c) Facade and side face of packaged MFC.

Table 1
Specifications of two types of multimode fibers (MMFs) with different numerical apertures (NAs) considered in study.

Fiber	Length (m)	Core diameter (μm)	Fiber diameter (μm)	NA	Refractive index of core/cladding
A	0.4	1470	1500	0.51	1.492/1.402
B	0.4	400	970	0.22	1.457/1.439

environment. Under changing environmental conditions such as MMF vibration, the power change in the ith guided mode, ΔP_i, can be expressed as

$$\Delta P_i = \sum_{j=1}^{M} h_{ij}(P_i - P_j), \tag{4}$$

where P_i and P_j represent the powers of the ith and jth guided modes, respectively. Further, h_{ij} denotes the coupling coefficient between modes i and j. In this regard, Kajenski et al. [26] have proposed a model to study the mode coupling in a fiber. If mode coupling occurs in the vibrating section of the fiber, the coupling coefficient can be expressed as

$$h_{ij} = \frac{1}{2}a^2\left\{K_{ij}\frac{L}{\pi}\cos\left[\frac{L(\beta_j - \beta_i)}{4}\right]\right\}^2 \cos(2\omega t), \tag{5}$$

where a and ω denote the amplitude and frequency of vibration, respectively, L the length of the fiber, K_{ij} a constant, and β_i and β_j the propagation constants of modes i and j, respectively.

According to Eq. (5), the mode coupling coefficient h_{ij} is proportional to the square of the amplitude a^2 of vibration. A change in the mode coupling coefficient results in a power change in each guided mode. Assuming that the total optical powers of all guided modes are equal over a certain integration time, these powers will be redistributed at the output of the MMF, which reduces the speckle noise. The greater is the change in the power of each mode, the smaller is the achieved speckle contrast [27]. Taking into account the number of all guided modes M, the speckle contrast at the output of the MMF can be written as [18]

$$C = \frac{1}{M\delta\tau}\left[2\int_0^{M\delta\tau}(M\delta\tau - \tau)|\gamma(\tau)|^2 d\tau\right]^{1/2} \tag{6}$$

where τ denotes the time delay between guide modes, $\delta\tau$ the time difference between the ith and the $(i-1)$th guided modes, and γ the complex degree of temporal coherence of the exciting source field. From Eqs. (4)–(6), it can be inferred that the mode coupling coefficient h_{ij} and number of guided modes M simultaneously influence the speckle contrast.

3.2. Experimental setup

Fig. 2 schematically shows our experimental setup to realize a low-coherence illumination light source using a combination of the MMF and MFC. A laser diode (LD, L520P50, Thorlabs) with 520 nm central wavelength is used as the laser light source. A linear polarizer is positioned after the LD to adjust the light intensity. The laser beam is coupled into the MMF through a fiber coupler with a coupling lens whose focal length is 4.6 mm. A diffuser made of sandblasted glass is positioned immediately after the MMF output to further scatter the light. The objective speckle patterns are captured by a CCD camera without a mounted imaging lens. The CCD camera has a resolution of 1280 × 1024 pixels, with the pixel size being 5.2 μm × 5.2 μm. Here we note that the MMF can be considered as a slack rope, with the two ends of the MFC glued firmly to the MMF with epoxy adhesive. A multifunction generator generates sinusoidal voltages, which are amplified by a high-voltage amplifier to drive the MFC and induce periodic vibration in the MMF.

In the study, the working temperature of the LD was maintained at 30 °C by means of a temperature-controlled mount, and the working current of the LD was set to 80 mA. Because speckles are sensitive to ambient influences such as external disturbances and background light, we placed the system on a stable optical table in a dark room to minimize the effects of these factors. The exposure time of the CCD camera was set at 30 ms, which is similar to the integration time of the human eyes. We captured speckle patterns for the two types of MMFs at different MFC driving frequencies and voltages. Here, we note that the configuration indicated by the dotted rectangle in Fig. 2 before the diffuser can be treated as a low-coherence illumination light source.

4. Experimental results and discussions

4.1. Effects of MFC driving frequency on speckle reduction

The relationship between the speckle contrast ratio and the MFC driving frequency is shown in Fig. 3. Error bar was given by calculating the standard deviations of the speckle contrasts of multiple measurements. Because the maximum working voltage of the MFC is 360 V under unipolar driving, and the high-voltage amplifier in our lab can generate an output voltage ranging from −150 V to 150 V (we note that the driving voltage "α V" refers the 0-to-α V peak-to-peak voltage in our study, where α denotes a constant.), we fixed the sinusoidal driving voltage at 100 V in consideration of the reliability of the high-voltage amplifier. The MFC driving frequency was varied from 0 to 200 Hz at 10 Hz intervals. The main reason for the driving frequency of the MFC being stopped at 200 Hz is that the typical integration time of human eyes is ~30 ms (~33.3 Hz). Because the speckle reduction mechanism of this method is by generating different speckle patterns and summing them together during the integration time of human eyes, the driving frequency of the MFC should be no less than ~33.3 Hz in order to use

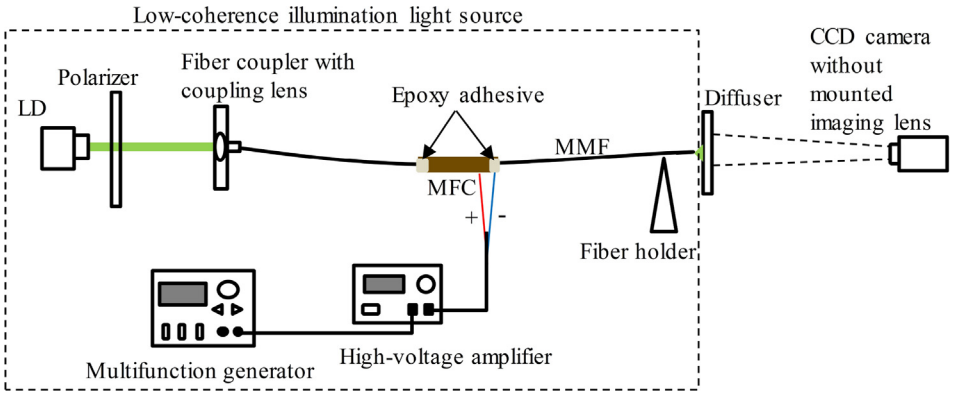

Fig. 2. Experimental setup to realize low-coherence illumination light source. A laser diode (LD) emits a beam whose intensity is adjusted by a linear polarizer. The polarized light is coupled into a multimode fiber (MMF) through a fiber coupler with a coupling lens to illuminate a diffuser. A macro fiber composite (MFC) is driven to induce periodic vibrations of the MMF, and objective speckle patterns are captured by a CCD camera without a mounted imaging lens.

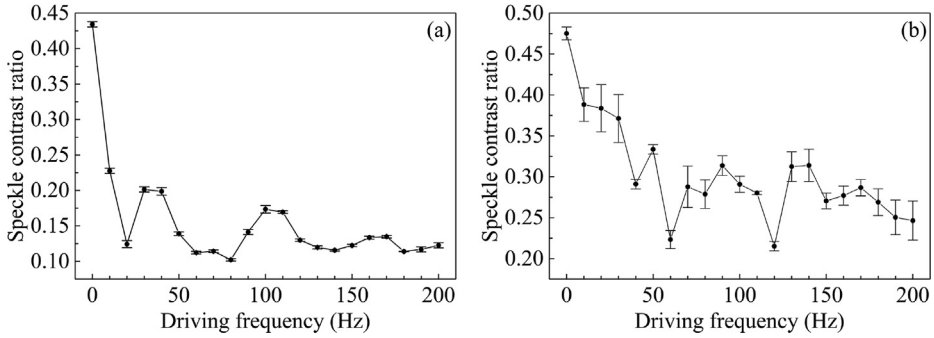

Fig. 3. Relationship between speckle contrast ratio and the macro fiber composite (MFC) driving frequency. The first two most efficient speckle suppression windows are observed at (a) ~20 Hz and ~80 Hz in fiber A and (b) ~60 Hz and ~120 Hz in fiber B when the fibers are vibrating in resonant modes.

all the generated different speckle patterns during one working period of the MFC. Therefore, resonant frequencies of the MMF larger than and closing to ~33.3 Hz are preferred, and higher resonant frequencies are not necessary though they can also be used. Speckle reduction was investigated under these driving conditions.

The speckle contrast ratios show a peak-and-valley variation as a function of the MFC driving frequency for both fibers A and B. Meanwhile, from Eqs. (4) and (5), we can infer that the deformation amplitude of the vibrating MMF influences the mode coupling coefficient, which is closely related to the speckle contrast. The MMF is forced into vibration by the MFC, and in terms of the vibration strength of the MMF, the MMF segment's vibration in the absence of the MFC is slight, which can be considered as stationary relative to the case when the MMF is connected to the MFC. Here, we note that only at the forced vibration frequency equal to the natural frequency of the MMF can the MMF reach the largest deformation (this driving frequency is the resonant frequency). From the figure, we note that the first two most efficient speckle suppression windows exist at ~20 Hz and ~80 Hz in fiber A and at ~60 Hz and ~120 Hz in fiber B. According to the principle of our speckle reduction method, vibration of the MMF results in the redistribution of optical powers at the output of the MMF, and hence, speckle patterns at the diffuser can be time-averaged over the exposure time of the CCD camera. The effective time-average of the speckle patterns corresponds to the power of each mode being varied on a time scale faster than the exposure time (30 ms) of the CCD camera. Therefore, we paid specific interest that the speckle contrast existed whenever the MFC driving frequency is greater than the driving frequency $f_i = 1/30\,\text{kHz} \approx 33.3\,\text{Hz}$. Thus, we focused on the speckle suppression window corresponding to ~80 Hz in fiber A. For consistency, we also studied the second most efficient speckle reduction window at ~120 Hz in fiber B. Here, we remark that the vibrating MMF can be considered as a free-free beam, whose resonant frequency f is given by [28]

$$f = \frac{k_n}{2\pi}\left(\frac{EI}{A\rho {L_b}^4}\right)^{1/2}, \tag{7}$$

where k_n is a coefficient of the nth resonant mode, E, I, ρ, and A represent the Young's modulus, second moment of area of the cross-section, density, and cross-sectional area of the beam, respectively, and L_b the length of the beam. In our study, the lengths L_b of the two beams (different vibrating MMFs, 100 mm) are identical. Because the two types of fibers are made of different materials, the Young's moduli E and densities ρ of the two beams are different. In addition, the second moments of area I and cross-sectional areas A are also unequal for the two beams due to the different fiber diameters. The resonant frequency for the beam when using fiber A is different from that when using fiber B, and it is determined by the abovementioned factors.

From Fig. 3, we note that when the MFC driving voltage is fixed at 100 V, the speckle contrasts reduce from $C_{off} = 0.43$ to $C_{on} = 0.10$ at 80 Hz for fiber A and from $C_{off} = 0.48$ to $C_{on} = 0.22$ at 120 Hz for fiber B. The most efficient speckle reduction situation corresponds to when the MMF is vibrating in a resonant mode. Here, we chose 80 Hz and 120 Hz as the optimized driving frequencies for fibers A and B, respectively, to suppress speckle noise.

4.2. Effect of MFC driving voltage on speckle reduction

In the next study phase, the driving frequency generated by the multifunction generator was fixed to the optimized value, and a sinusoidal driving voltage was amplified by means of the high-voltage amplifier to drive the MFC. Considering the ability of the high-voltage amplifier in our lab, the maximum driving voltage of the MFC was stopped at 150 V in this measurement. Fig. 4 shows the relationships between the speckle contrast ratio, speckle reduction efficiency, and the MFC driving voltage.

From Fig. 4, the stationary speckle contrast when using fiber A ($C_{off} = 0.43$) is lower than that when using fiber B ($C_{off} = 0.48$) without vibration. In our study, the diameter of the laser emitted from the LD is ~ 3 mm measured by means of a beam profiler, and the coupling lens has a 4.6 mm focal length, the effective numerical aperture is $NA_e = n_0 \times \sin\theta = 1 \times ((3/2)/((3/2)^2 + 4.6^2)^{1/2}) \approx 0.31$, where n_0 represents the refractive index of air, this NA_e is smaller than the actual NA of fiber A but larger than that of fiber B from Table 1, thus, the effective NA_es of fibers A and B are $NA_e = 0.31$ and $NA_e = 0.22$, respectively. According to Eqs. (2) and (3), the lengths of fibers A and B are identical, the time difference $\Delta\tau$ in fiber A is larger than that in fiber B. Therefore, a lower speckle contrast can be produced in fiber A relative to fiber B. We also note that the speckle contrast exhibits an

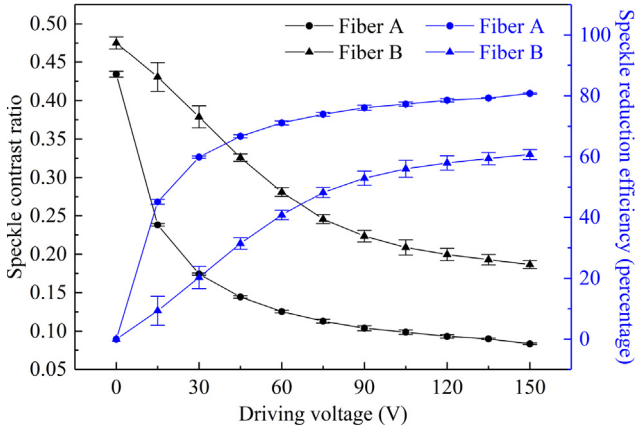

Fig. 4. Relationships between speckle contrast (black line), speckle reduction efficiency (blue line), and the macro fiber composite (MFC) driving voltage for fiber A (circles) and fiber B (triangles) under the optimized frequencies. (For interpretation of the references to color in this figure legend, the reader is referred to the web version of this article.)

overall decrease with increase in the driving voltage for both fibers A and B. Here, it is noteworthy that in both cases, the speckle contrast ratios show saturation trends; this can be attributed to the MFC special strain characteristic. The relationship between the MFC strain and driving voltage shows nonlinear: when the MFC is subjected to low driving voltages, its strain is approximately proportional to the driving voltage, and the MFC strain tends to saturation due to the saturation polarization of the piezoelectric rod as the driving voltage increases [29]. These properties firstly lead to greatly increased deformation of the MMF, which then tends to saturation; this explains the resulting trend of speckle contrast ratio in Fig. 4. Moreover, the speckle reduction efficiency of fiber A is obviously greater than that of fiber B at the same driving voltage. Here, we define speckle reduction efficiency as $(C_{off} - C_{on})/C_{off}$. From Eqs. (4)–(6), in addition to noting that the change in the mode coupling coefficient h_{ij} results in reduced speckle contrast, we also note that the speckle contrast C is also inversely proportional to the number of guided modes M. The number of modes supported by a MMF is given by $M \approx \pi d(NA_e)/\lambda$ [6], where d and λ represent the MMF core diameter and the wavelength of the laser light, respectively. The NA_e and core diameter d of fiber A are larger than the corresponding ones of fiber B, thus modes in fiber A outnumber the modes in fiber B. Therefore, the larger number of modes propagating in fiber A affords greater speckle reduction efficiency. Here, we remark that the optimized driving conditions are 80 Hz, 150 V for fiber A and 120 Hz, 150 V for fiber B.

4.3. Discussion

Fig. 5 shows the speckle patterns captured by the CCD camera in the no-vibration and vibration scenarios under optimized driving conditions for the two fibers; the significant speckle reduction between the two scenarios is clearly visible even with the naked eyes. The speckle contrasts reduce from $C_{off} = 0.43$ initially to $C_{on} = 0.08$ for fiber A and from $C_{off} = 0.48$ initially to $C_{on} = 0.19$ for fiber B under the optimized conditions.

From Fig. 5(a) and (c), we note that the speckle size formed on the CCD camera when using fiber B is larger than that when using fiber A with the MFC turned off. The relationship between the speckle size (diameter) D_s and diameter D_c of the coherence light corresponding to a circular region on the diffuser can be expressed as $D_s \approx 1.2\lambda s/D_c$, where s denotes the distance between the diffuser and the CCD camera [30]. In our setup, the distances $s = 0.37$ m are identical for fibers A and B. Because the diffuser is positioned immediately beyond the MMF output, the smaller core diameter of fiber B relative to fiber A results in a smaller diameter D_c of coherence light on the diffuser, which generates a larger speckle size on the CCD camera.

In a previous study, it has been reported that when individual speckle reduction mechanisms are compounded, speckle contrast C can reduce from $C = 1$ to $C = 1/N_s^{1/2}$, where $N_s = (1/C)^2 = \Pi N_i$ represents the total degree of speckle reduction freedom, and N_i the speckle reduction freedom introduced by the ith speckle reduction mechanism [7]. In our study, the factors contributing to speckle reduction included the modal dispersion N_d of the stationary MMF, the time-averaging effect N_t of the vibrating MMFs during the exposure time of the CCD camera, and the independent orthogonal polarizations N_p due to multiple scatterings of the diffuser. Under the optimized driving conditions, the total degree of the speckle reduction freedom N_s were $N_s = (1/C_{on})^2 = (1/0.08)^2 \approx 156$ for fiber A and $N_s = (1/C_{on})^2 = (1/0.19)^2 \approx 28$ for fiber B. The temporal degree of speckle reduction freedom due to MMF vibration during the exposure time can be calculated as $N_t = (C_{off}/C_{on})^2$, and in our study, these results were $N_t = (0.43/0.08)^2 \approx 29$ for fiber A and $N_t = (0.48/0.19)^2 \approx 6$ for fiber B. Here, we find that the factors $N_d \times N_p = N_s/N_t = (1/C_{off})^2$ are $N_d \times N_p = (1/0.43)^2 \approx 5$ for fiber A and $N_d \times N_p = (1/0.48)^2 \approx 4$ for fiber B, wherein $N_t > N_d \times N_p$ in the two fibers. These results indicate that the time-averaging effect due to the vibrating MMFs during the exposure time of the CCD camera is the dominant factor among the three individual speckle reduction mechanisms. In future, we plan to optimize the combination of the MMF and the MFC and use other resonant frequencies and different types of MFCs to reduce speckle more efficiently.

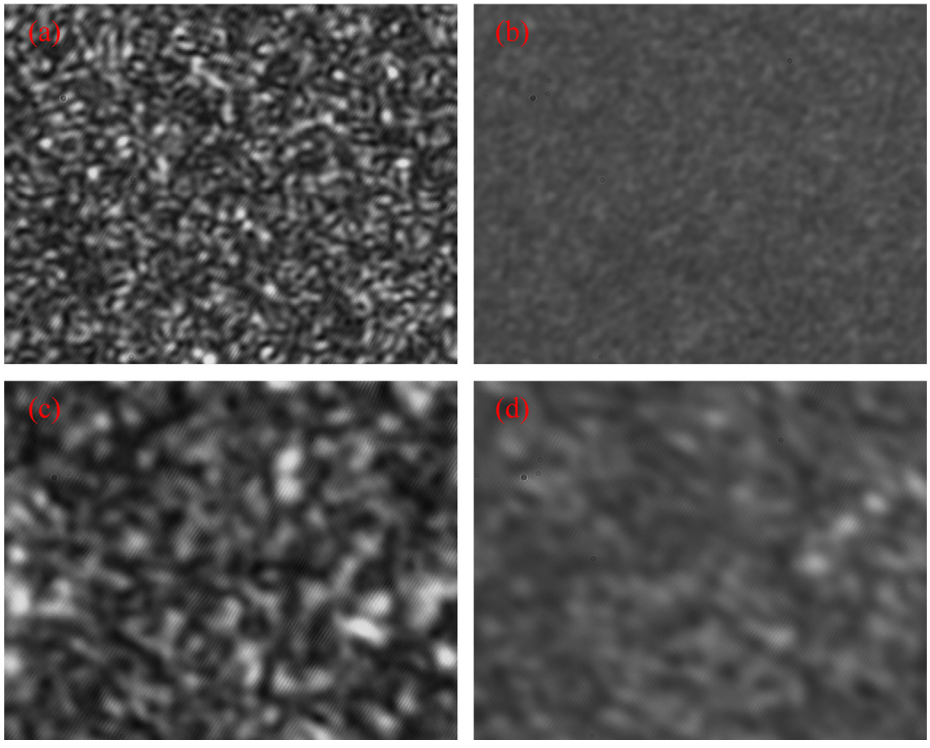

Fig. 5. Speckle patterns with macro fiber composite (MFC) (a) turned off, with speckle contrast ratio $C_{off} = 0.43$, and (b) turned on under the optimized conditions (80 Hz, 150 V), with speckle contrast ratio $C_{on} = 0.08$ for fiber A and with MFC (c) turned off, with speckle contrast ratio $C_{off} = 0.48$, and (d) turned on under the optimized conditions (120 Hz, 150 V), with speckle contrast ratio $C_{on} = 0.19$ for fiber B.

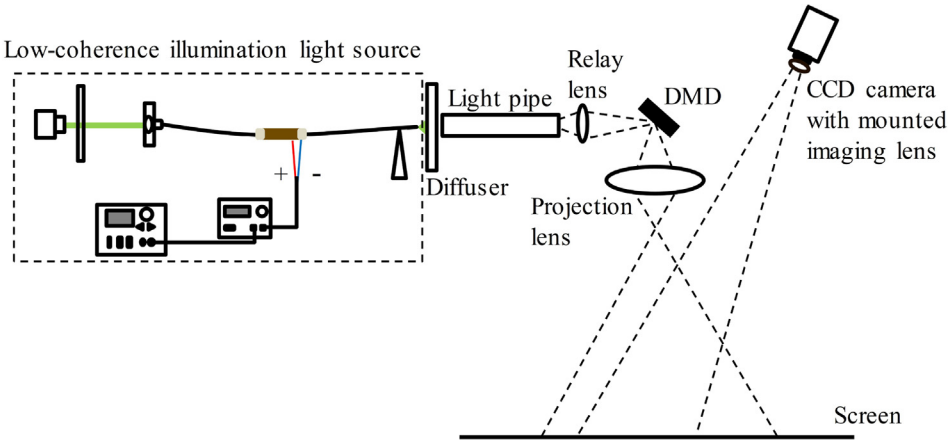

Fig. 6. Low-coherence illumination light source used in simplified projection system. The low-coherence light illuminates a digital micromirror device (DMD) though a diffuser, light pipe, and relay lens. The modulated light is guided to the screen by means of a projection lens. The projection images are captured by a CCD camera with a mounted imaging lens.

5. Application in laser projector

Next, to verify the feasibility of our speckle reduction module in laser projection displays, we set up a simplified projection system [8]. In order to achieve greater speckle reduction, we used fiber A in the proposed configuration as a low-coherence illumination light source in the simplified projection system. The conceptual diagram of this setup is shown in Fig. 6.

In the setup, the low-coherence light emerging from the proposed configuration is homogenized by means of a diffuser and a light pipe to illuminate a digital micromirror device (DMD) through a relay lens. The modulated light is directed to a screen through a projection lens. A CCD camera with a mounted imaging lens that has the equivalent function of human eyes is used to capture the projection images, wherein the lens is adjusted to ensure that it always focuses the image on the screen. In our study, to increase the brightness of the projection images, the working current of the LD was set at 150 mA and the linear polarizer was adjusted to ensure maximum light transmission. The distances between the screen and projection lens and between the CCD camera and the screen were set to 0.7 m and 1.2 m, respectively. The other conditions were the same as those corresponding to Fig. 2. The above-mentioned optimized driving conditions (80 Hz, 150 V) were applied to the MFC to investigate the speckle reduction effect in the laser projector. Fig. 7 shows the resulting projection images and the relationships between the grayscale of the cross section of the projection image and the CCD camera pixel in the vibration-off state and the vibration-on state.

When the MFC is in the vibration-off state, the image exhibits strong speckles (Fig. 7(a)), whereas the image shows barely any speckle when the MFC is turned on (Fig. 7(b)). The white horizontal stripes appearing in the enlarged area in Fig. 7(b) correspond to the details of the rough screen captured by the CCD camera. From the results, we can verify that the MMF vibration forms the dominant principle underlying this speckle reduction system, and the less fluctuated grayscale line shown in Fig. 7(d) indicates that the output beam becomes increasingly uniform with MMF operation. Our results further indicate that the proposed speckle reduction method using a combination of the MMF and the MFC is feasible and that our flexible and lightweight module can be easily integrated in the proposed low-coherence illumination light source in laser projection displays to suppress speckle noise.

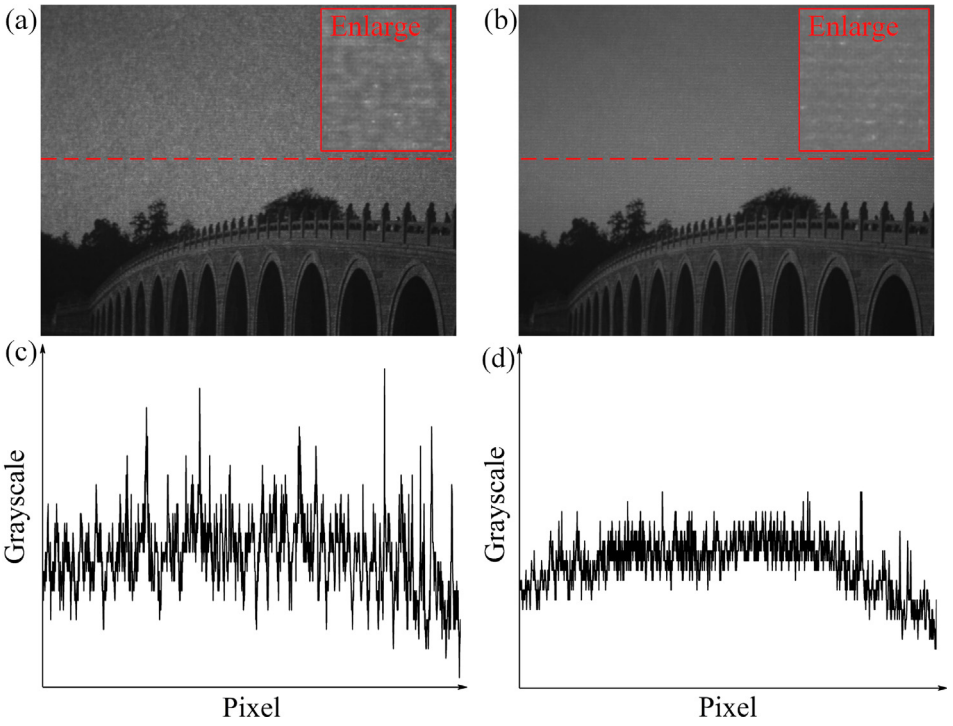

Fig. 7. Projection images before (a) and after (b) introducing the MFC vibration under the optimized driving conditions. Relationships between the grayscale of the cross section of the projection image (red dotted lines in (a) and (b)) and the CCD camera pixel in the vibration-off state (c) and the vibration-on state (d). (For interpretation of the references to color in this figure legend, the reader is referred to the web version of this article.)

6. Conclusions

We experimentally studied the performance of a flexible and lightweight speckle reduction module based on the combination of a MMF (two types: fibers A and B with different NA values) and a MFC, wherein the MFC was used as a driver to vibrate the MMF. The consequent redistribution of powers at the output of MMF resulted in speckle reduction at the diffuser. Moreover, the speckle patterns were captured and speckle contrasts were calculated for analysis. We achieved the most efficient speckle reduction when the MMF was vibrating in a resonant mode and the MFC driving voltage was maximal. Under these conditions, the speckle contrasts reduced from 0.43 to 0.08 for fiber A and 0.48 to 0.19 for fiber B. Further, we used the proposed low-coherence illumination light source in a laser projection display, and in the resulting high-quality projection images, speckles were hardly visible. In future, we plan to determine a more efficient speckle reduction configuration by optimizing the MFC. We believe that our flexible and lightweight speckle reduction module can be extended to many laser application fields.

Declaration of Competing Interest

The authors declared that there is no conflict of interest.

Acknowledgments

This research was supported by the National Key Research and Development Program of China (2016YFB0401903), the Key Research and Development Program of Shanxi Province for International Cooperation (201703D421015), the Changjiang Scholars and Innovative Research Team in University of Ministry of Education of China (IRT_17R70), the State Key Program of National Natural Science of China (11434007), the 111 project (D18001), and the Fund for Shanxi “1331 Project” Key Subjects Construction.

References

[1] V. Kartashov, M.N. Akram, Speckle suppression in projection displays by using a motionless changing diffuser, J. Opt. Soc. Am. A 27 (12) (2010) 2593–2601.
[2] V. Yurlov, A. Lapchuk, K. Han, S. Son, B.H. Kim, N.E. Yu, Binary code DOE optimization for speckle suppression in a laser display, Appl. Opt. 57 (30) (2018) 8851–8860.
[3] Y. Zhang, H. Dong, R. Wang, J. Duan, A. Shi, Q. Fang, Y. Liu, Demonstration of a home projector based on RGB semiconductor lasers, Appl. Opt. 51 (16) (2012) 3584–3589.
[4] W.C.Y. Lo, N. Uribe-Patarroyo, A.S. Nam, M. Villiger, B.J. Vakoc, B.E. Bouma, Laser thermal therapy monitoring using complex differential variance in optical coherence tomography, J. Biophoton. 10 (1) (2017) 84–91.
[5] R.K. Tyson, Adaptive optics and ground-to-space laser communications, Appl. Opt. 35 (19) (1996) 3640–3646.
[6] J.W. Goodman, Speckle Phenomena in Optics: Theory and Applications, Roberts and Company Publishers, Englewood, CO, 2006.
[7] Z. Tong, W. Shen, S. Song, W. Cheng, Z. Cai, Y. Ma, L. Wei, W. Ma, L. Xiao, S. Jia, X. Chen, Combination of micro-scanning mirrors and multi-mode fibers for speckle reduction in high lumen laser projector applications, Opt. Express 25 (4) (2017) 3795–3804.
[8] Q. Ma, C.Q. Xu, A. Kitai, D. Stadler, Speckle reduction by optimized multimode fiber combined with dielectric elastomer actuator and lightpipe homogenizer, J. Disp. Technol. 12 (10) (2016) 1162–1167.
[9] Z. Tong, X. Chen, Speckle contrast for superposed speckle patterns created by rotating the orientation of laser polarization, J. Opt. Soc. Am. A 29 (10) (2012) 2074–2079.
[10] D.S. Mehta, D.N. Naik, R.K. Singh, M. Takeda, Laser speckle reduction by multimode optical fiber bundle with combined temporal, spatial, and angular diversity, Appl. Opt. 51 (12) (2012) 1894–1904.
[11] G. Ouyang, M.N. Akram, K. Wang, Z. Tong, X. Chen, Laser speckle reduction based on angular diversity induced by Piezoelectric Benders, J. Eur. Opt. Soc.-Rapid 8 (2013).
[12] J. Kinoshita, H. Aizawa, A. Takamori, K. Yamamoto, H. Murata, K. Tojo, Angular dependence of screen speckle and fiber speckle of coupled output of nine high-power blue laser diodes through a multi-mode fiber, Opt. Rev. 23 (1) (2016) 121–132.
[13] H. Yamada, K. Moriyasu, H. Sato, H. Hatanaka, Effect of incidence/observation angles and angular diversity on speckle reduction by wavelength diversity in laser projection systems, Opt. Express 25 (25) (2017) 32132–32141.
[14] B. Redding, P. Ahmadi, V. Mokan, M. Seifert, M.A. Choma, H. Cao, Low-spatial-coherence high-radiance broadband fiber source for speckle free imaging, Opt. Lett. 40 (20) (2015) 4607–4610.
[15] N.E. Yu, J.W. Choi, H. Kang, D.K. Ko, S.H. Fu, J.W. Liou, A.H. Kung, H.J. Choi, B.J. Kim, M. Cha, L.H. Peng, Speckle noise reduction on a laser projection display via a broadband green light source, Opt. Express 22 (3) (2014) 3547–3556.
[16] C.Y. Chen, W.C. Su, C.H. Lin, M.D. Ke, Q.L. Deng, K.Y. Chiu, Reduction of speckles and distortion in projection system by using a rotating diffuser, Opt. Rev. 19 (6) (2012) 440–443.
[17] J. Pauwels, G. Verschaffelt, Speckle reduction in laser projection using microlens-array screens, Opt. Express 25 (4) (2017) 3180–3195.
[18] P. Hlubina, Spectral and dispersion analysis of laser sources and multimode fibres via the statistics of the intensity pattern, J. Mod. Opt. 41 (5) (1994) 1001–1014.
[19] A. Efimov, Coherence and speckle contrast at the output of a stationary multimode optical fiber, Opt. Lett. 43 (19) (2018) 4767–4770.
[20] J.G. Manni, J.W. Goodman, Versatile method for achieving 1% speckle contrast in large-venue laser projection displays using a stationary multimode optical fiber, Opt. Express 20 (10) (2012) 11288–11315.
[21] D. Furman, D. Mandelik, Speckle reduction using a fiber bundle and light guide, U. S. Patent Application 11/503, 859, 2008.
[22] W.S. Ha, S.J. Lee, K.H. Oh, Y. Jung, J.K. Kim, Speckle reduction in near-field image of multimode fiber with a piezoelectric transducer, J. Opt. Soc. Korea 12 (3) (2008) 126–130.
[23] Y. Fujimaki, H. Taniguchi, Reduction of speckle contrast in multimode fibers using piezoelectric vibrator, Proc. SPIE 8960, 89601S, 2014.
[24] https://www.smart-material.com/MFC-product-main.html.
[25] A. Pandey, A. Arockiarajan, Fatigue study on the sensor performance of macro fiber composite (MFC): Theoretical and experimental approach, Compos. Struct. 174 (2017) 301–318.
[26] P.J. Kajenski, P.L. Fuhr, D.R. Huston, Mode coupling and phase modulation in vibrating waveguides, J. Lightwave Technol. 10 (9) (1992) 1297–1301.
[27] W. Ha, S. Lee, Y. Jung, J.K. Kim, K. Oh, Acousto-optic control of speckle contrast in multimode fibers with a cylindrical piezoelectric transducer oscillating in the radial direction, Opt. Express 17 (20) (2009) 17536–17546.
[28] C.L. Kirk, S.M. Wiedemann, Natural frequencies and mode shapes of a free–free beam with large end masses, J. Sound Vib. 254 (5) (2002) 939–949.
[29] L.J. Nelson, Smart piezoelectric fibre composites, J. Mater. Sci. Technol. 18 (11) (2002) 1245–1256.
[30] A. Ennos, J.C. Dainty (Eds.), Speckle interferometry, in: Laser Speckle and Related Phenomena, Springer-Verlag, 1975.